Wind and Structures, *Vol. 42, No. 2 (2026) 281-302*
https://doi.org/10.12989/was.2026.42.2.281

Techno-Press

Wind-induced tree collapse along railways: An approach to mesoscale mapping of risk index with application

Lorenzo Raffaele*, Elisabetta Colucci[a], Luca Bruno[b]

GeoWindy R&D group, Department of Architecture and Design, Politecnico di Torino, Viale Mattioli 39, Torino, 10126, Italy

(Received January 23, 2025, Revised April 1, 2025, Accepted April 15, 2025)

Abstract. Wind-induced tree collapse on critical infrastructures, such as railway lines, results from the interaction between wind in the Atmospheric Boundary Layer, tree aerodynamics and mechanics, and specific features of the infrastructure. Wind-induced tree collapse may affect railway capacity and safety. The resulting losses may be related to delays, cancellations, or even damages caused to the infrastructure or the rolling stock. In order to face the potential adverse events above, risk analysis provides a sound methodological framework to infer critical railway segments referring to the main risk determinants: wind hazard, tree and railway exposure, and tree vulnerability to wind. Each risk determinant has and can be modelled at multiple scales in space and or time. The risk assessment should effectively model hazard, exposure, and vulnerability at a selected scale that is consistent across all three determinants and relevant to the context of interest. In this study, a mesoscale approach is proposed to assess and map the relative risk level of different railway segments along a line or within a network. Wind hazard index is grounded on the extreme wind speed mapping obtained by the Authors by means of a reanalysis-based approach. Tree exposure index is defined on the basis of land cover characteristics. Tree vulnerability index is defined with reference to the critical wind speed for tree collapse. Each index and the resulting risk is mapped by Geographic Information System tools. The Calabria region in Southern Italy is selected as a challenging benchmark due to its variable orography and due to the wide presence of railway lines surrounded by tree canopies both in coastal and mountainous zones. The proposed mesoscale approach allows to identify in quantitative relative terms the most endangered railway segments over the region of interest.

Keywords: GIS; mesoscale; railway infrastructure; risk; tree collapse; wind hazard

1. Introduction

The engineering scientific interest about wind-induced tree collapse is driven by its harmful interactions with built structures and infrastructures, such as roads and railways, power lines, towns, and single buildings. Wind storms represent a key external forcing factor for European forests, causing uprooting or breaking of trees. On the one hand, wind-induced damage to trees is classified as the major physical disturbance in European forest ecosystems [1] both to date and for

*Corresponding author, Ph.D., Assistant Professor, E-mail: lorenzo.raffaele@polito.it
[a] Ph.D., Assistant Professor
[b] Ph.D., Professor

http://www.techno-press.org/was/5
ISSN: 1226-6116 (Print), 1598-6225 (Online)

the foreseeable future [2] impacting both ecosystems services and the surrounding economy [3]. On the other hand, many studies assume that the increment of atmospheric moisture due to global warming will lead to high-energy storms [4], leading to an increment of wind-induced tree collapse events along infrastructures [5].

Wind-induced tree collapse induces detrimental effects on both urban environment and infrastructures. Urban forestry is increasingly acknowledged as a valuable tool for city planners to enhance air quality, reduce noise pollution, mitigate the urban heat island effect, and manage rainwater runoff within urban areas [6]. Nevertheless, tree collapse may cause injuries or deaths, representing a detrimental effect on human safety [7]. Along railway infrastructures, fallen trees may cause traffic disruption due to their collapse on rails and/or on the overhead power line. The resulting losses are considered indirect when they pertain to train traffic disruptions, leading to consequences such as delays, rescheduling, or even cancellations. Indirect costs are typically incurred by the infrastructure provider, primarily in the form of fines and an increase in compensation claims from the public due to periods of infrastructure downtime [8]. Conversely, direct losses and costs are associated to the removal of the collapsed tree and the repair of any damage caused to the infrastructure or the rolling stock, eventually leading to train derailment and casualties [9]. Significant direct and indirect losses induced by tree collapses have been reported in many European countries, among which United Kingdom [10], Finland [11], Sweden [12], Poland [13], Czech Republic [9], and Germany [14].

Wind-induced tree collapse is a multi-physics phenomenon, resulting from the interaction between wind flow aerodynamics and tree mechanics, and a multi-scale phenomenon, spanning from the microscale of tree-level fluid-structure interactions and infrastructure components (tens of meters scale), to the mesoscale of tree canopies, single infrastructures and meteorological phenomena such as thunderstorms, sea breezes, and medicanes (kilometers scale), and further extending to the macroscale of forests, infrastructure networks and large-scale meteorological systems like weather fronts (thousands of kilometers scale).

Although wind-induced tree collapse along infrastructures has serious implications on human safety and infrastructure operation, the formulation of the problem within a comprehensive risk analysis framework is still uncommon, with some recent remarkable exceptions. According to the authors, such a framework should involve the definition of the determinants influencing the risk being assessed, i.e., wind hazard, tree exposure, tree vulnerability to wind, and infrastructure exposure, at a consistent selected scale of observation. Bil et al. [15] define the risk as the probability of tree collapse within a 50 m distance from the railway track. The risk is assessed at the microscale (100 m resolution along track) exploiting available historical data on tree falls along railway lines, while the modelling of wind hazard and tree vulnerability are disregarded. Hughes [15] define risk as the probability of a tree falling and striking an infrastructure. They propose a methodological framework to assess interruptions of several infrastructures (transportation network, power distribution system, and residential buildings) because of tree collapse, where wind hazard is considered at the macroscale by setting it constant over the whole region of interest, while tree exposure and tree vulnerability are considered at the microscale through single tree fragility curves. Gullick et al. [8] and Szymczak et al. [16] conceive a comprehensive risk analysis framework based on the estimation of wind hazard at the mesoscale (5 km resolution in [8]) and microscale (200 m resolution in [16]) based on interpolated wind speed datasets from meteorological stations, while tree exposure and vulnerability are defined at the microscale considering individual tree simplified geometry and mechanical characteristics. In Gullick et al. [8], risk is defined as a function of the difference between the estimated wind speed

intensity and critical wind speed for stem breakage or uprooting, and the distance from the infrastructure, while in Szymczak et al. [16], risk is defined through fuzzy logic as a function of soil type, wind speed, tree height and vitality, and distance from the railway track. Gardiner et al. [14] define the probability of tree collapse through a logistic function comparing the predicted wind speed with the critical one. They develop a wind-induced tree collapse mapping tool taking into account wind hazard at the mesoscale (about 2.2 km resolution) resulting from the refinement of ERA5 reanalysis data by adopting the regional climate model COSMO-CLM [17], while the exposure and vulnerability of nearly 2 million individual trees are defined at the microscale after LiDAR flights, in analogy with [8].

According to the brief state-of-the-art outlined above, the authors identify two main concerns. First, the definition of risk is not uniform among the cited publications. Depending on the study, risk can be defined in terms of (i) a dimensionless index, (ii) the probability of tree collapse in the neighborhood of the infrastructure, or (iii) the product between the probability of tree collapse and the probability of striking. Secondly, the modelling of risk determinants is not uniform in terms of the considered scale in space and time. Wind hazard is typically characterized at the macro- or, at best, mesoscale, whereas tree exposure and vulnerability are defined at the microscale. From one side, this implies that the resulting risk is constrained by the coarsest spatial resolution among its constituent determinants. On the other side, the collection of a huge amount of data of individual trees is not compliant with preliminary design and risk assessment of nation-wide infrastructure networks.

Within this spirit, the present study proposes a new fully consistent mesoscale approach for the mapping of the risk index of wind-induced tree collapse along railways. The dimensionless quantitative risk index allows to define risk in relative terms over the considered region, allowing for the identification of critical railway segments along which mitigation measures should be implemented, or around which risk could eventually be downscaled in the wake of a supplementary microscale study. Wind hazard, tree exposure and tree vulnerability are defined at the mesoscale with a common horizontal resolution of about 2.2 km. Such a high resolution is made possible thanks to the novel Italian extreme wind speed map recently proposed in Raffaele et al. [18]. The proposed mesoscale approach is then applied and tested in a real-world benchmark.

The paper is organized into three further sections. In Sect. 2, the layout of the mesoscale risk modelling framework is introduced by discussing in detail each determinant affecting risk. In Sect. 3, adopted datasets are introduced and the proposed risk modelling framework is applied on a case study. Finally, conclusions and perspectives are outlined in Sect. 4.

2. Modelling framework

In the following, the proposed methodological framework to assess the risk of wind-induced tree collapse along railway infrastructures is introduced.

According to the definition provided by intergovernmental panel on climate change [19], risk is defined as the "*the likelihood over a specified time period of severe alterations in the normal functioning of a community or a society due to hazardous physical events interacting with vulnerable social conditions, leading to widespread adverse human, material, economic, or environmental effects that require immediate emergency response to satisfy critical human needs and that may require external support for recovery*". Within this framework, in the present study risk is defined in relative terms over the region of interest by conceiving a dimensionless risk

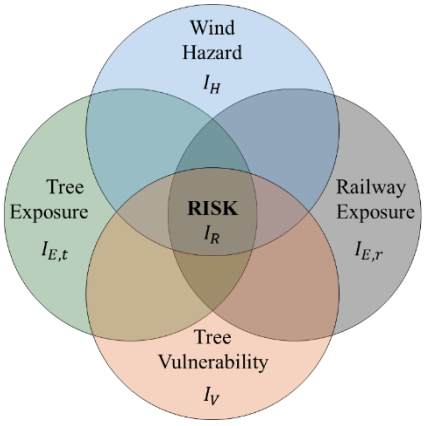

Figure 1. Methodological framework to assess the risk of wind-induced tree collapse along railway lines

index accounting for railway disruptions due to wind-induced tree collapse.

The risk of railway line disruption is defined as a function of four determinants: wind hazard, tree exposure, railway exposure, and tree vulnerability (see Fig. 1). Wind hazard describes extreme wind speed. Exposure describes the amount and location of the natural or built assets at risk in the region of interest. In particular, exposure of tree canopies and railway line defines the location and typology of such assets. Tree vulnerability results from the sensitivity of tree canopies to wind hazard. As a result, the dimensionless risk index I_R can be defined through the following multiplicative formula

$$I_R := I_H \cdot I_V \cdot I_{E,t} \cdot I_{E,r} \,, \tag{1}$$

where:

• the wind hazard index I_H, bounded between [0,1], is expressed as the normalized extreme wind speed with return period T_r over the whole analysed territory;

• the tree vulnerability index I_V is defined as a dimensionless variable bounded between [0,1] proportional to the sensitivity of wind canopies to wind hazard;

• the tree exposure index $I_{E,t}$ is a logical variable expressing the geographical location of tree canopies per each hazardous event;

• the railway exposure index $I_{E,r}$ is defined along the alignment as a dimensionless variable bounded between [0,1] proportional to the physical exposure of each railway segment to tree collapse.

In the next Subsections wind hazard, tree vulnerability and exposure are discussed in detail and their indices are defined.

2.1 Wind hazard

The determination of design wind speeds forms the foundational and critical element of the "Alan G. Davenport Wind Loading Chain" which continues to underpin modern Wind Engineering [20-21]. Traditionally, the design wind speed for a given site is obtained through a

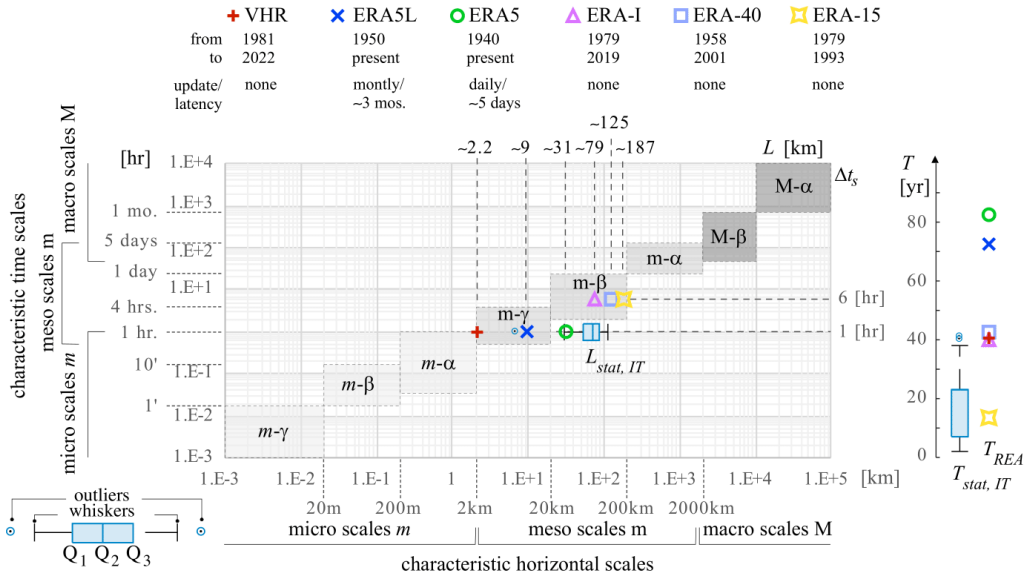

Figure 2. Space and time scales of the atmospheric processes, synopsis of the time series duration, horizontal resolution and sampling period of the reanalysis models [REA, specifically ERA-15, ERA-40, ERA-Interim (ERA-I), ERA5, ERA5-Land (ERA5L), VHR-REA_IT (VHR)], and of the Italian land anemometric stations used in [22].

two-stage, fourth-and-back approach between different spatial scales. In the first stage, synoptic extreme wind speeds are zoned at the macroscale resolution (spanning hundreds of kilometers) on the basis of extreme value statistical analysis of time series from land-based anemometric stations. This process involves data acquisition, correction, transformation, and their statistical analysis (see Ballio et al. [22] for application to Italy). The resulting climatic wind zoning, developed at the national scale, are incorporated into engineering standards (e.g., [23-24] for Italy). Conversely, the second stage is directly handled by the designer through the so-called "return criterion" [22]. This step involves adapting the reference wind speed provided by the maps to calculate the design wind speed. The adaptation accounts for site-specific and construction-related characteristics, such as altitude above sea level, aerodynamic roughness, orography, proximity to the shoreline, and the reference height. The 'map-and-return' approach has been originally conceived to allow the setting of the design wind speed at a given individual construction site, rather than to provide a comprehensive map over a spanned territory of the wind hazard expressed by its Intensity Measure (IM). In addition, both of the stages described above are affected by some weaknesses pointed out by e.g., [18]. The critical issues in the map stage stem directly from the quantity and quality of the available anemometric measurements, namely the spacing of ground-based measurement stations, the duration of the time series, the local characteristics of each station's installation site, and the specifications of the measuring instruments. The critical issues in the return stage indirectly reflect those encountered during the map phase, requiring the designer to model the specific characteristics of the project site and their effects on the wind field. Among these, we recall the subjective and challenging assessment of the aerodynamic roughness z_0, the variations between different terrain categories and the corresponding z_0 values in standards, and the estimation of the effects of the local terrain orography.

The Authors have very recently proposed in [18] a new approach called REA-*ha* able to both map without gaps the wind hazard IM throughout a Country (first 'REAnalysis' stage), and hence to specify the design wind speed at every construction site and height from the ground (second '*h*eight *a*djust' stage). In the following, the REA stage is recalled, being the one relevant to wind hazard.

The REA stage takes advantage of refined climate models, their reanalysis through satellite observations, their downscaling via regional climate models, and extreme values analysis to finally gather extreme wind speeds at 10-meter height corresponding to different values of the return period. Fig. 2 maps the average horizontal and temporal resolutions of European Centre for Medium-Range Weather Forecasts (ECMWF) and Centro Euro-Mediterraneo sui Cambiamenti Climatici (CMCC) REA models onto the space and time scales of atmospheric processes, as initially defined in meteorology [25] and widely recognized in Wind Engineering [26].

Since the release of the first global reanalysis in 1997 (ERA-15) to the most recent in 2023 (ERA5, [27]), ECMWF models have progressively improved their horizontal resolution from approximately $L \approx 187$ km to $L \approx 31$ km, thus spanning the entire range of meso-β scales. Similarly, the temporal resolution has advanced from 6-hourly wind speed data (meso-β time scale in ERA-15, ERA-40, and ERA-Interim) to 1-hourly data (meso-γ time scale in ERA5), while the historical time series have extended from $T = 14$ year in ERA-15 to $T = 83$ years in ERA5. Various methods for regional downscaling of reanalysis data have been proposed, and seldomly adopted to wind engineering and namely critical infrastructures (e.g., [28]). Among them, Fig. 2 includes ERA5-Land reanalysis (ERA5L) and the Very High Resolution REA over Italy (VHR) by CMCC [29].

For comparison, Fig. 2 also highlights the horizontal resolution $L_{stat,IT}$ and time series duration $T_{stat,IT}$ of the anemometric stations used to map extreme wind speeds in Italy. While ERA5, ERA5L, and VHR match the sampling period of these stations, they offer longer time series and higher spatial resolution, fully covering the meso-γ scale. In Raffaele et al. [18], it has been shown that VHR can resolve the meso-γ scale, capturing wind variations in areas with discontinuous roughness and orographic complexity. VHR has been derived from the VHR dynamical downscaling of ERA5 reanalysis to the so-called convection-permitting scale [29]. The regional downscaling covers a domain around Italy (lon 5°:20°E, lat 36°:48°N) with a horizontal resolution equal to $\theta = 0.02°$, i.e., about 2.2 km. Convection-permitting regional climate models are increasingly attracting attention within the climate science community due to their demonstrated ability to simulate precipitation characteristics with greater accuracy and sensitivity to climate change [44]. Additionally, their enhanced horizontal resolution significantly improves the representation of fine-scale features, such as complex orography and transitions in surface roughness, particularly in coastal zones and urban areas.

The proposed approach offers several conceptual and technical advantages compared to the currently codified method. During the reanalysis stage: (i) there is no need for transformations across scales or the processing of non-homogeneous and scattered data; (ii) all effects, including the orographic ones, are consistently and explicitly accounted for up to the mesoscale, while microscale effects are intentionally and explicitly excluded; (iii) the high horizontal resolution in space and the continuous sampling in time provide detailed "gap-free" maps of wind speed and aerodynamic roughness. Despite these advantages, it should be noted that the REA-based extreme wind speed modeling tends to underestimate measured values for increasing values of the return period T_R. As a result, REA-based extreme wind speed estimates shall be adjusted by means of a suitably tuned model correction factor, as detailed in [18]. The REA extreme wind speed

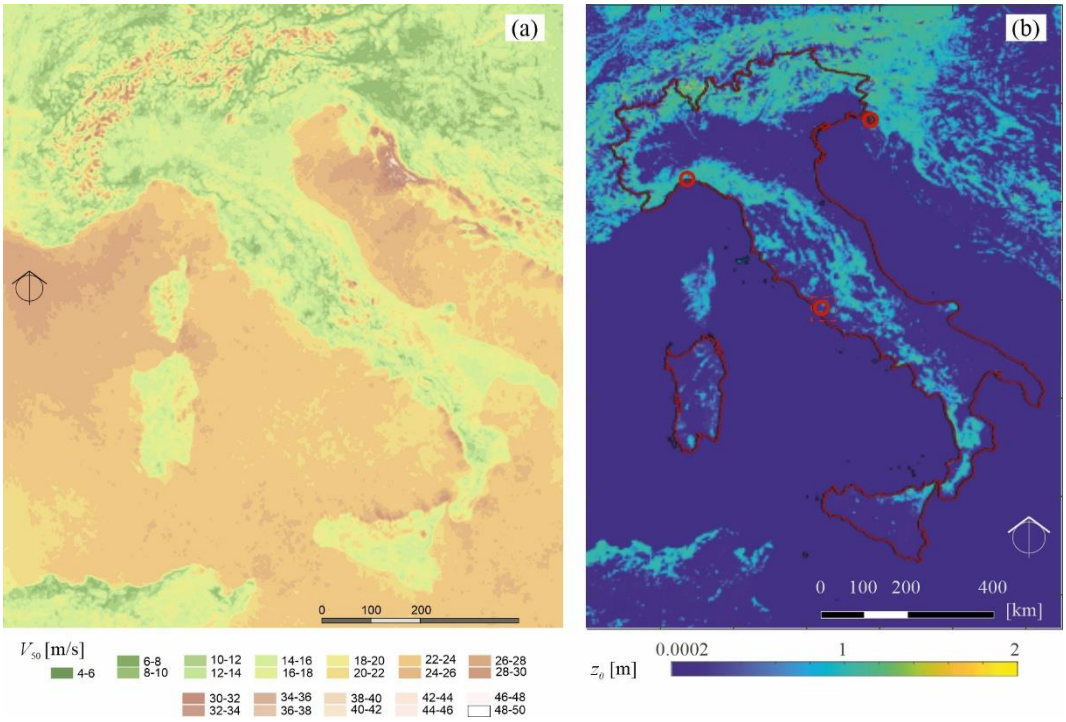

Figure 3. Map of the extreme wind speed V_{50} with return period T_R= 50 years (a). Mapping of z_0 according to VHR (b, courteously provided by CMCC Foundation)

can then be expressed in correspondence of the cell of longitude x and latitude y as

$$V_{T_R}(x,y) = \gamma_{m,T_R} V_{REA,T_R}(x,y) \,, \tag{2}$$

where γ_{m,T_R} is the model correction factor, V_{REA,T_R} is the mapped wind speed from REA stage defined at the standard reference height $z_{ref} = 10$ m, and with a return period T_R. In the following, the extreme wind speed at 10 m height V_{50} for a 50-year return period is adopted based on standard practices in Wind Engineering applications.

Fig. 3(a) shows the Italian map of V_{50} resulting from the statistical processing of about 163.5 billion wind speed data at 444,000 VHR cells (horizontal resolution equal to about 2.2 km).

The high spatial resolution of V_{50} map provides a significantly more detailed depiction of extreme wind speeds compared to the current wind speed zoning provided in the Italian standard [23-24].

Largest wind speed magnitudes are observed over water bodies, such as seas and lakes, due to their low aerodynamic roughness, and along mountain ridges, where strong orographic effects are directly incorporated. In absolute terms, the highest wind speeds in the analyzed domain occur along the Croatian coastline near the Velebit mountain range, a region well-documented in the literature for generating intense Bora winds [31]. On the Italian side, particularly windy areas are identified at the Strait of Bonifacio due to the channeling effect between northern Sardinia and southern Corsica, and along the Tyrrhenian coasts of Sicily and Calabria, where the complex orography behind the shoreline plays a significant role. Fig. 3(b) shows z_0 from VHR dataset as

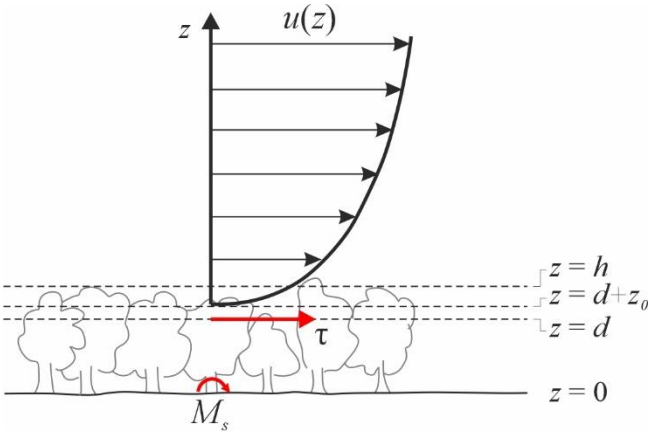

Figure 4. Wind speed profile $u(z)$ and shear stress τ above a tree canopy (redrawn after Dyrbye and Hansen 1997)

the sum of the roughness associated to subgrid-scale variance of orography according to GLOBE Digital Elevation Model [32] and the roughness associated to the land-use category according to GLC2000 [33]. In other words, the z_0 map includes the effects induced by both natural (e.g., tree canopies) and built (e.g., urban canopies) diffused obstacles.

Finally, the dimensionless wind hazard index I_H is then defined with respect to the once in 50-year wind speed at 10 m height as

$$I_H(x,y) := \frac{V_{50}(x,y)}{\max[V_{50}]}. \tag{3}$$

It follows that $I_H \in [0,1]$ by definition and will be maximum and equal to 1 in correspondence of the cell of longitude x and latitude y with largest extreme wind speed over the analysed area.

2.2 Tree vulnerability

Vulnerability can be defined as the susceptibility of natural or built assets to be damaged by the hazard. In a general risk analysis framework, and in analogy with seismic risk analysis [34], vulnerability can be described through (i) fragility curves, expressing the probability of attaining damage as a function of the hazard intensity; (ii) damage probability matrices, representing the conditional probability of obtaining different damage levels given the hazard intensity; or (iii) vulnerability curves, representing the variation of a mean value of damage with the hazard intensity.

From a Structural Engineering perspective, existing approaches to account for tree vulnerability to wind are still far to be homogenously integrated into a robust and comprehensive risk analysis framework. In general terms, three main damage mechanism can be identified: (i) stem breakage or (ii) tree overturning if the wind-induced drag force on the tree crown multiplied by the lever-arm results in a bending moment exceeding the bending resistance of the stem or the root anchorage, respectively (see e.g., [35]); and (iii) branch breakage, when the wind-induced drag force on the tree branch multiplied by the lever-arm results in a bending moment exceeding the bending resistance of the branch itself (see e.g., [36]). To the authors' best knowledge, approaches

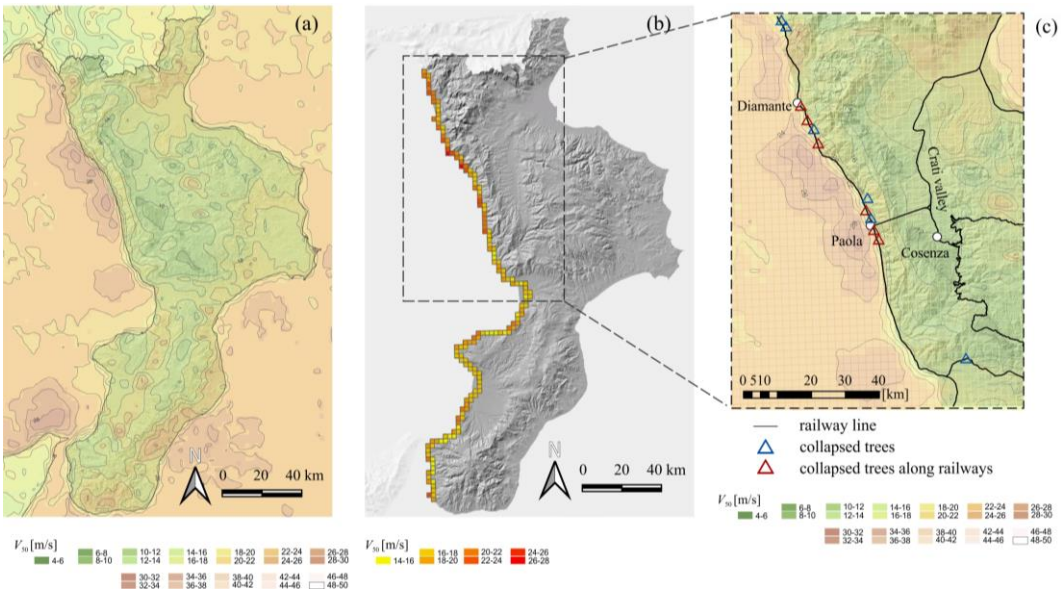

Figure 5. Mesoscale map of the extreme wind speed V_{50} in Calabria (a), V_{50} at cells along the Tyrrhenian railway line (b), closeup view of the map around the zone surrounding Diamante and Paola with censused tree collapse events (c)

for the definition of tree vulnerability to wind hazard can be categorized into so-called *mechanistic models* defined e.g., by [37-39], and *finite element models*, developed e.g., by [40-43]. It is worth mentioning that tree fragility curves have been recently developed considering uncertainties in tree strengths, morphologies, and loadings. Nevertheless, the former are the most widespread approaches to tree vulnerability given their analytical formulation relating wind-induced bending moment to the stabilizing one in order to assess the critical wind speed for stem breakage and tree overturning. Branch breakage is seldom considered when accounting for tree vulnerability (see e.g., [44].

In the following branch failure is neglected, given the extremely localized nature of the scale of the phenomenon, and the approach proposed by Gardiner et al. [38] has been considered since it allows to focus on a tree canopy rather than on a single tree. In other words, it can be easily adapted to assess tree vulnerability at the mesoscale rather than on the microscale. The resistant bending moments M_r for breakage $M_{r,b}$ and overturning $M_{r,o}$ can be defined through the simple relations:

$$M_{r,b} = \frac{\pi \sigma_y \phi^3}{32}, \tag{4}$$

$$M_{r,o} = W C_o, \tag{5}$$

where σ_y is the green wood yielding strength, ϕ is the stem diameter, W is the tree total weight and C_0 is a semi-empirical coefficient obtained from tree pulling experiments, function of tree species, soil type and rooting depth.

According to Gardiner et al. [38] the mean bending moment M_s at the height $z = 0$ depends on the wind-induced mean shear stress over the canopy τ, and on the average spacing between trees D (see Fig. 4) through the relation

$$M_s = d\tau D^2, \tag{6}$$

where d is the height of the zero displacement plane. By substituting $\tau = \rho u_*^2$, and assuming a log-law wind speed profile above the tree canopy we can then obtain the bending moment M_s

$$M_s = \rho d \left(\frac{D u_{10} k}{\ln \frac{10}{z_0}} \right)^2 \tag{7}$$

where ρ is the air density, u_* is the average wind shear velocity, k is the von Karman's constant, u_{10} is the average wind speed at 10 meter height. By equating Eq. 7 with Eq. 4 and Eq. 5, we can then assess the critical wind speed at canopy 10 meter above the zero displacement plane for stem breakage and overturning:

$$u_c(x,y) = \sqrt{M_r} \cdot \frac{1}{D\sqrt{\rho}} \cdot \sqrt{\frac{1}{d}} \cdot \frac{\ln \frac{10}{z_0}}{k}, \tag{8}$$

where $M_r = M_{r,b}$ or $M_r = M_{r,o}$.

It is worth stressing that Eq. (8) highlights the multi-scale nature of tree vulnerability. On the one hand, the critical wind speed depends on mesoscale tree canopy features, i.e., tree spacing (D), canopy height (d) and roughness (z_0). On the other hand, it depends on microscale features contributing to the resistant moment M_r of each individual tree, i.e. wood yielding strength σ_y, stem diameter ϕ, tree weight W, soil type and rooting depth C_0 (see e.g., [38]).

The mesoscale tree vulnerability dimensionless index I_V is then defined as

$$I_V(x,y) := \frac{\max[u_c] - u_c(x,y)}{\max[u_c]}. \tag{9}$$

In this study, vulnerability is evaluated at the mesoscale by neglecting the spatial variability of microscale tree/terrain features. In other words, the resistant moment M_r is set constant in space so that it simplifies and no longer holds in Eq. (9). The tree canopy features, i.e. tree spacing (D), canopy height (d) and roughness (z_0) are obtained by available global maps at native mesoscale resolution, in order to avoid ad hoc local field surveys of the individual trees, e.g., by aerial photogrammetry or LiDAR measurements. The surface roughness z_0 is directly obtained from the mesoscale VHR mapping (Fig. 3(b)). The roughness in correspondence of shoreline cells whose centroid falls into water bodies (i.e., sea and lakes) is set equal to $z_0 = 0.1h$, in agreement with [45-46], in order to assign to those cells the roughness of the tree canopy. The tree spacing $D = 1/\sqrt{\gamma}$ is estimated from the tree density γ map generated at global scale by [47] using satellite imagery with horizontal resolution of 1 km. The height of the tree canopy displacement plane $d = 2/3h$ is estimated from the canopy height h in agreement with [45-46]. The 10 m high-resolution global map of the canopy height h is drawn by Lang *et al.* [48] using Sentinel-2 satellite imagery. Both γ and h datasets are oversampled at the horizontal resolution of 2.2 km, consistently with z_0. $I_V \in [0,1]$ by definition and will be maximum in correspondence of tallest canopies with lowest densities (i.e., largest displacement d and tree spacing D), and minimum and equal to 0 in

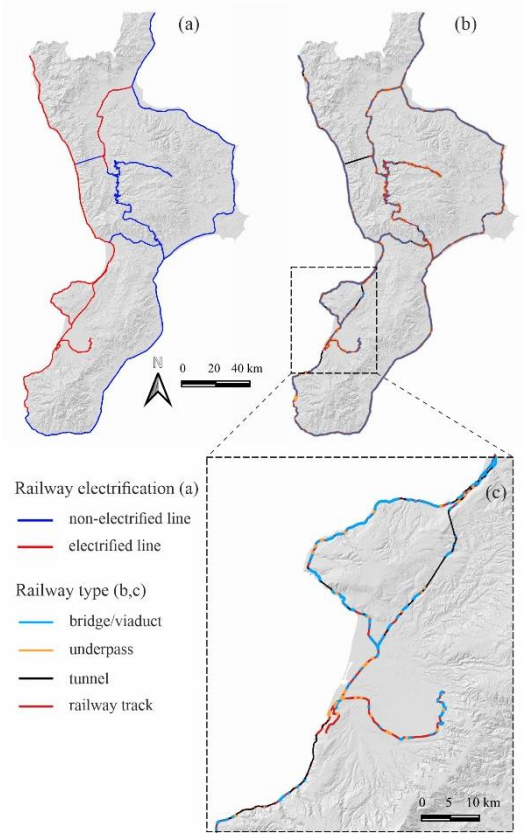

Figure 6. Calabria railway network: electrified lines (a), railway infrastructure type (b,c)

correspondence of the shortest, most dense canopies.

2.3 Tree exposure

The tree exposure index $I_{E,t}$ is derived from the satellite high-resolution maps of European land cover from CORINE inventory (CLC [49] horizontal resolution of 100m). In particular, CLC categories Broad-leaved forest (311), Coniferus forest (312), and Mixed forest (313) are considered. The horizontal resolution of the tree exposure is oversampled at 2.2 km, ensuring consistency with the resolution of I_H. As such, the tree exposure is set equal to $I_{E,t} = 1$ at (x, y) corresponding to forests while $I_{E,t} = 0$ elsewhere. It is worth stressing that only tree canopies with $h \geq 2$ m are retained. As such, the tree exposure in correspondence of cells with average tree height $h < 2$ is set equal to $I_{E,t} = 0$.

3. Application and results

In the following, the modelling framework introduced in Sect. 2 is applied to a benchmark case study. The Calabria region in Southern Italy is selected as a particularly challenging benchmark

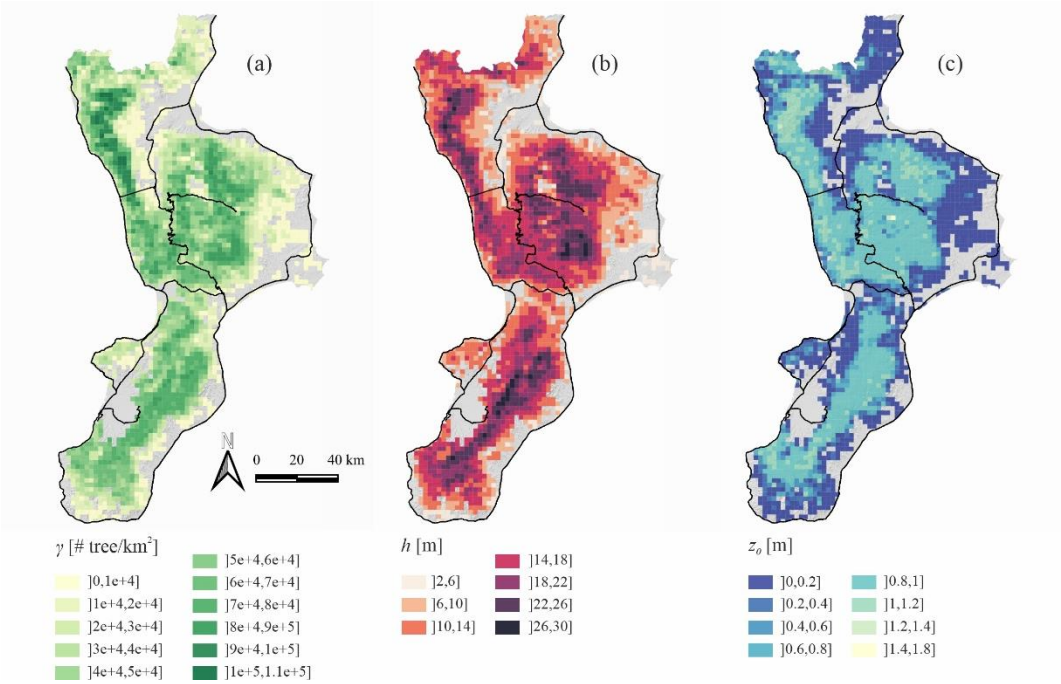

Figure 7. Mesoscale maps of tree canopy mean density γ (a), mean height h (b), and surface roughness z_0 (c) with common horizontal resolution $L = 2.2$ km according to [47], [48] and [29], respectively

due to its geomorphological characteristics, marked by widespread roughness and highly variable orography across extensive coastal and mountainous areas, and due to the wide presence of railway lines surrounded by tree canopies both in coastal and mountainous zones.

3.1 Data sources and preprocessing

The wind hazard index I_H is assessed through Eq. (2) and (3) over Calabria thanks to the extreme wind speed mapping over the whole Italian territory carried out by the authors in [18]. Fig. 5(a) plots extreme wind speed over Calabria region. Largest wind speed magnitudes are observed along the northern Tyrrhenian coast. As an example, Fig. 5(b) highlights extreme wind speed at VHR cells crossed by the Tyrrhenian railway line in Calabria while Fig. 5(c) provides a closeup view of the map around the zone surrounding the Tyrrhenian coast around Diamante and Paola with censused tree collapse events. Effects induced by orography and aerodynamic roughness can be exemplified: (i) along the Crati valley, close to Cosenza wind speed is low due to the high roughness associated to the urban canopy and the sheltering effect provided by mountain ridges; (ii) wind speed increases along the northern part of the valley due to the lower roughness and its opening towards the Calabrian east coast; (iii) wind speed is very high along the Tyrrhenian coast due to the steep orography and the very low aerodynamic roughness of the water surface. Over the same closeup view, some recent events reported in the press of trees collapse due to strong winds are georeferenced [50-54]. Most of them are localized along the Tyrrhenian coast due to the high mesoscale extreme wind speed, and in some cases affecting the railway line operation.

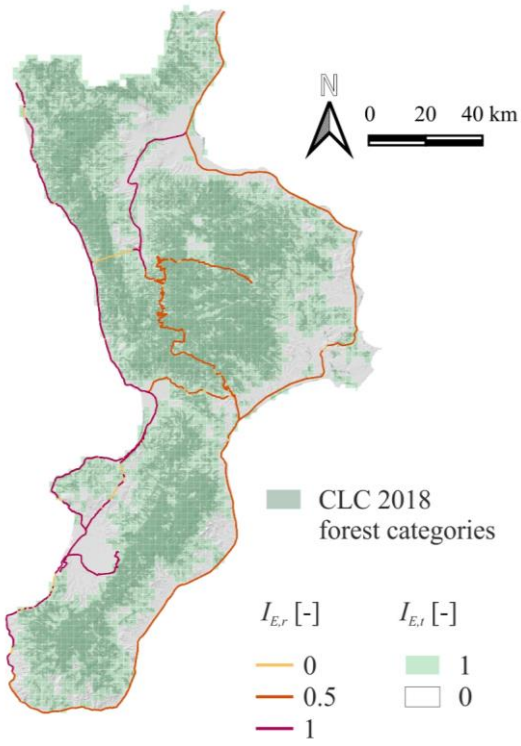

Figure 8. Tree canopy exposure index $I_{E,t}$ according to CLC 2018 categories and railway exposure index $I_{E,r}$ according to railway electrification and type

Railway exposure is georeferenced through the Italian railway network published on the Italian Geoportal (https://gn.mase.gov.it) updated to the year 2008. The railway network discerns line segments depending on the presence of the overhead power line (Fig. 6(a)) and the railway infrastructure type, i.e. tunnel, underpass, viaduct, bridge, and railway track (Figs. 6(b)-6(c)). It is worth stressing that the available railway network does not discern between different railway body types, e.g., embankment and cutting. Accordingly, the physical exposure of the railway line is defined as $I_{E,r} = 1$ along electrified railway segments, reflecting their higher exposure to tree collapse, as falling trees frequently inflict substantial damage on overhead lines [16], $I_{E,r} = 0.5$ along non-electrified railway track because of their moderate exposure to tree collapse, and $I_{E,r} = 0$ along tunnel, underpass, viaduct and bridge railway infrastructures because of their nil exposure to tree collapse.

The tree vulnerability index $I_{V,t}$ is assessed adopting Eq. (8) and (9). The spatial mapping of the tree density γ, canopy height h and roughness z_0 is plotted in Fig. 7 over Calabria in correspondence of the cells for which $I_{E,t} = 1$. The spatial pattern of γ, h, and z_0 is analogous: the boundaries of forested zones have lower tree density, height, and roughness, while they all increase in inner forested zones.

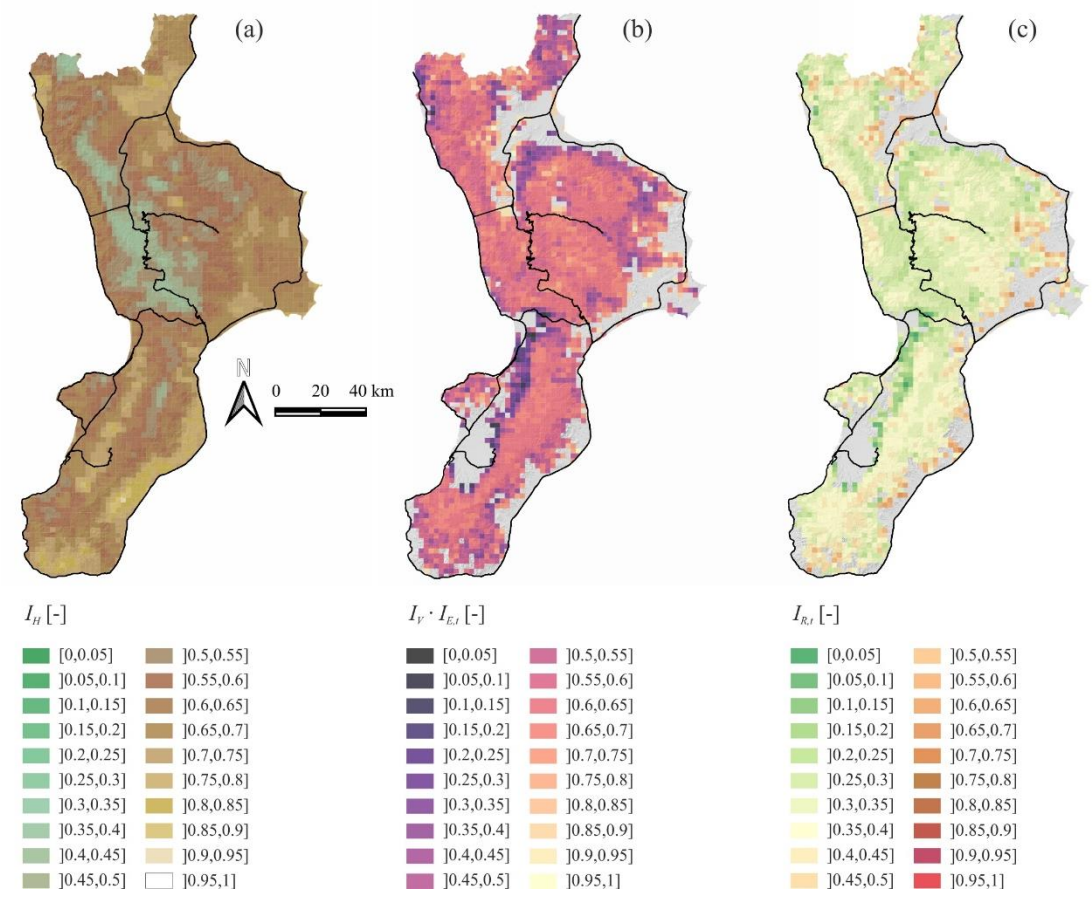

Figure 9. Mesoscale maps of wind hazard index I_H (a), tree vulnerability index I_V in correspondence of $I_{E,t} = 1$ (b), and wind-induced tree collapse risk index $I_{R,t}$ (c) over Calabria region

3.2 Results

In the following, tree and railway exposure indices, wind hazard index, tree vulnerability index, and risk index are mapped over the Calabria region and their spatial variability is critically discussed.

Fig. 8 shows the mapping of the tree canopy exposure index $I_{E,t}$ superimposed to the railway exposure index $I_{E,r}$.

It is worth highlighting that cells for which $I_{E,t} = 1$ comprehend and circumscribe land surface for which the land cover according to [49] is classified as forest. We can notice that the Tyrrhenian coastal railway line (west coast) has an higher exposure than the Ionic coastal one (east coast) because of the electrification of the former. Inland railway lines are predominantly non-electrified, giving rise to an intermediate railway exposure despite the presence of significant forested zones.

The assessment of wind-induced tree collapse risk across Calabria integrates wind hazard, tree vulnerability, and exposure. The resulting tree collapse risk is shaped by the interplay of these

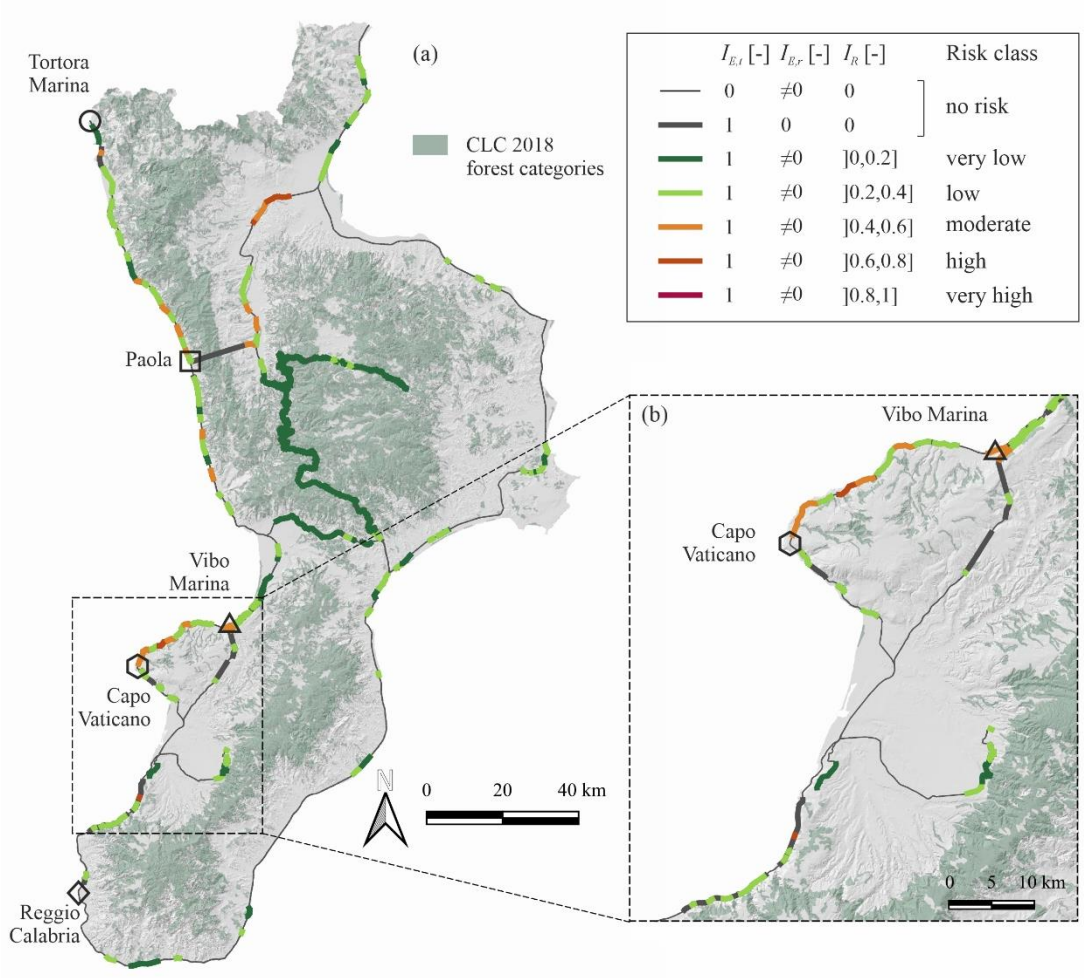

Figure 10 Map of wind-induced tree collapse risk index I_R along Calabria railway network (a). Closeup view of the map along the Tyrrhenian coast between Capo Vaticano and Messina Strait (b)

factors, heavily influenced by the region's complex orography and forest characteristics. Fig. 9 includes the mapping of the hazard index I_H (Fig. 9(a)), tree vulnerability index I_V (Fig. 9(b)) in correspondence of cells for which the tree exposure is equal to 1 (i.e. $I_V \cdot I_{E,t}$), and the resulting wind-induced tree collapse risk index $I_{R,t} = I_H \cdot I_{E,t} \cdot I_V$ (Fig. 9(c)).

Calabria's rugged terrain, dominated by mountain ranges such as the Sila, Aspromonte, and Serre, combined with extensive forest cover, explains the variability in wind hazard and vulnerability. High wind hazard is observed along exposed ridges and slopes, areas where the topography amplifies wind speed magnitude, and in correspondence of sea, lakes and over flat open terrain, due to their low roughness. Conversely, low wind hazard occurs in correspondence of valleys due to their wind sheltering effect. The vulnerability index integrates structural and aerodynamic characteristics of the trees. Taller trees are primarily found in the dense, high-elevation forests of central and southern Calabria (Figs. 7(a)-7(b)). High roughness values correspond to densely forested zones (Fig. 7(c)), indicating increased shear stress that can

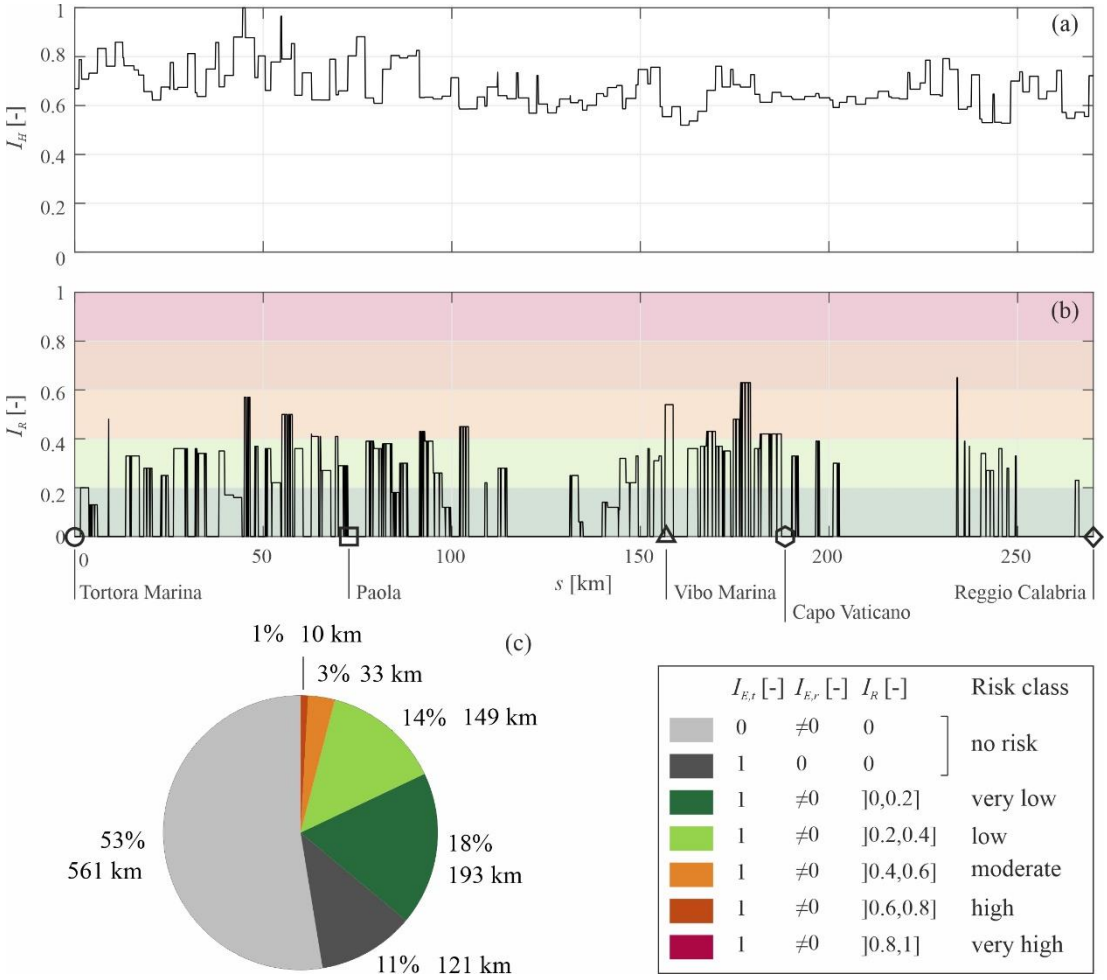

Figure 11 Wind hazard index I_H (a) and wind-induced tree collapse risk index I_R (b) long the Tyrrhenian railway alignment. Pie chart of the Calabrian railway network showing the distribution of total kilometers by risk class (c)

exacerbate tree vulnerability to strong winds. In general, trees vulnerability to wind (Fig. 9(b)) largely depends to their spatial distribution and height, i.e., I_V is low at the edge of forested zones with sparse, shorter trees and it is higher within the core of forested areas where trees are denser and taller. I_V attains largest values in local, isolated cells, in the case of canopies with tall, sparse trees, especially at the edge of forested zones. The tree collapse risk index map (Fig. 9(c)) shows high-risk areas where wind hazard aligns with vulnerable and exposed forests. The tree collapse risk index $I_{R,t}$ pattern largely follows the one of $I_V \cdot I_{E,t}$ because of the broader variation of I_V with respect to I_H. As a result, the high-risk zones are most prominent at the edge of forested zones, including the west coastal strip facing the Tyrrhenian Sea.

The wind-induced tree collapse risk index along railway lines is depicted in Fig. 10(a) along the whole Calabrian railway network, resulting from the product between the tree collapse risk index of the crossed cell and the railway segment exposure, i.e., $I_R = I_{R,t} \cdot I_{E,r}$.The land zones classified

as forests according to [49] are highlighted for reference. The resulting risk is then categorized into 6 risk classes, as a function of the I_R value. In particular the "no risk" class refers to railway segments along which $I_R = 0$ because of $I_{E,t} = 0$ (thin black line), i.e. nil tree exposure due to absence of tree canopies within the crossed cell, or $I_{E,r} = 0$ (thick grey line), i.e., nil railway exposure due to railway track crossing tunnels, viaducts or underpasses. For illustrative purpose, Fig. 10(b) shows a closeup view of the map along the Tyrrhenian coastal railway between Vibo Marina and Messina Strait allowing to appreciate the fine-grained succession of risk classes. The Tyrrhenian railway line running from Tortora Marina, at the Calabria northern border, to Reggio Calabria results to be overall the most prone to wind-induced tree collapse. The Ionic railway line, facing the east coast, scores at most low/very low risk along a few railway segments due to the scarcity of tree canopies. Similarly, the inland railway lines mainly score low/very low risk because of the sheltering effect of valleys (see e.g., railway lines crossing the centre of Calabria), except some local moderate/high risk railway segments crossing flat, open terrain lands in northern Calabria, due to the presence of localized small vulnerable canopies.

Given the larger sensitivity of the Tyrrhenian coastal railway line to tree collapse, Fig. 11(a)-11(b) plot the values of hazard and risk indices along the railway alignment cumulative curvilinear distance s spanning from Tortora Marina to Reggio Calabria. Wind hazard results higher and bounded between $I_H = [0.6,1]$ along the first 100 kilometres, locally reaching the peak $I_H = 1$ in correspondence of $s \approx 45\text{km}$ before decreasing between I_H=[0.5,0.8] from $s \approx 100$ km up to Reggio Calabria. Similarly, the vast majority of railway segments at risk are concentrated along the first 100 kilometres, even if the largest I_R is attained locally between Vibo Marina and Capo Vaticano ($175 < s < 180$ km) and between Capo Vaticano and Reggio Calabria (namely at $s = 233$ km) because of the larger tree vulnerability.

Finally, Fig. 11(c) comprehensively aggregate in a pie chart the overall curvilinear length of railway track of the whole Calabrian 1067 km-long railway network categorized into each risk class. In general, the vast majority (64%) of railway lines are not at risk because of nil tree exposure (53%) or nil railway exposure (11%). Among railway lines exposed to wind-induced tree collapse risk, the vast majority are classified as subjected to low/very low risk (342 km, i.e., 32%), while just 44 kilometers (4%) are classified at moderate/high risk. In a comprehensive regional network-wide risk assessment framework, information as the ones in Fig. 11(b) and Fig. 11(c) allow railway owners/managers/designers to identify the location and overall length of railway segments prone to wind-induced tree collapse in order to (i) synthetically quantify the overall risk of the railway network; (ii) prioritize the inspection and maintenance, or the installation of mitigation measures designed to locally reduce the risk by lowering the wind hazard, tree vulnerability, and/or exposure; (iii) eventually plan microscale risk assessment studies to refine the mesoscale risk analysis to the scale of the individual trees, or to account for localized, i.e. with $L \leq 2.2$ km, changes in orography or railway type, e.g., deep and narrow gorges with steep slopes, or short span bridges or tunnels, respectively.

4. Conclusions

In the present study, an approach to mesoscale mapping of wind-induced tree collapse risk along railway infrastructures is proposed.

Wind hazard, tree exposure, tree vulnerability, and the resulting risk of tree collapse are all modelled through dimensionless indices, uniformly defined at the lower bound of the meso-γ scale

spatial resolution (about 2.2 km). Wind hazard index results from the reanalysis-based mapping of the extreme wind speed over the whole Italian territory proposed in [18]. Tree exposure index is defined as a logical variable expressing the presence or absence of tree canopies within the area of interest. Tree vulnerability index results from the mesoscale mapping of the critical wind speed for tree breakage/overturning disregarding tree microscale mechanical features. Finally, the wind-induced tree collapse risk along railway is defined per each railway segment as the product between the risk of tree collapse and the exposure of the railway line.

The proposed approach is then applied to a benchmark case study dealing with the wind-induced tree collapse risk assessment along the Calabrian railway network. This demonstrates the soundness of the approach in identifying most endangered railway segments. It is worth stressing that, even if the risk is not defined in probabilistic terms through the probability of failure, the dimensionless risk index allows to identify in quantitative relative terms the most endangered railway segments over the region of interest. Within this framework, the proposed approach allows railway owners, managers and designers to localize and discern most critical railway segments along which (i) prioritize and plan the implementation of maintenance protocols and/or design of mitigation measures with the aim of decreasing the local risk through the reduction of wind hazard, tree vulnerability, and/or exposure; (ii) carry out microscale risk assessment studies based on microscale Computational Wind Engineering simulations to refine mesoscale wind speed, and local assessment of the single trees mechanical properties.

In the wake of the discussed mesoscale approach, the authors suggest the following research perspectives. First, in the same proposed framework, railway exposure could be further improved to account for other railway body types (i.e., embankment/cutting), their height/depth from the ground, the intrinsic value of the exposed asset, and the consequences of its failure over the whole network. Secondly, the downscaling at microscale would allow the definition of risk in full probabilistic terms through the assessment of the probability of failure. This implies the reformulation of wind hazard in terms of probability of exceedance, and of tree vulnerability in terms of fragility curves for each class of trees, accounting for the uncertainty in tree spacing, height, aerodynamic and mechanical characteristics. Thirdly, the comprehensive collection and classification of wind-induced tree collapse events would allow to validate the proposed model. Fourthly, based on the probabilistic definition of risk, the approach could be expanded to estimate indirect costs induced by tree collapse over railway networks. Finally, the proposed framework can be readily adapted to address similar engineering challenges, such as tree falls along pipelines, roads, and overhead powerlines (e.g., [55]).

Acknowledgments

This study was carried out within the RETURN Extended Partnership and received funding from the European Union Next-GenerationEU (National Recovery and Resilience Plan – NRRP, Mission 4, Component 2, Investment 1.3 – D.D. 1243 2/8/2022, PE0000005) – SPOKE TS 2. This study was jointly developed in the framework of the research project PROtection Technologies from Eolian Events for Coastal Territories (PROTEECT, http://www.proteect.polito.it/) within the Ministerial Decree no. 1062/2021 and received funding from the FSE REACT-EU - PON Ricerca e Innovazione 2014–2020. This manuscript reflects only the authors' views and opinions, neither the European Union nor the European Commission can be considered responsible for them. The Authors thank F. Giulio Tonolo and F. Rinaudo, members of the GeoWindy R&D group

(https://geowindy.polito.it) at the Department of Architecture and Design - Politecnico di Torino, for the stimulating discussions about the general topic of the study. This study would have not been possible without the huge research effort paid by the European Centre for Medium-Range Weather Forecasts (ECMWF), the Copernicus European programme, and the Euro-Mediterranean Centre on Climate Change (CMCC), and without the datasets VHR-REA_IT (https://doi.org/10.25424/cmcc/era5-2km_italy) and CORINE Land Cover 2018 (https://doi.org/10.2909/71c95a07-e296-44fc-b22b-415f42acfdf0) made available in Open Access.

References

1. Patacca, M., Lindner, M., Lucas-Borja, M. E., Cordonnier, T., Fidej, G., Gardiner, B., Hauf, Y., Jasinevičius, G., Labonne, S., Linkevičius, E., Mahnken, M., Milanovic, S., Nabuurs, G.-J., Nagel, T. A., Nikinmaa, L., Panyatov, M., Bercak, R., Seidl, R., Ostrogović Sever, M. Z., Socha, J., Thom, D., Vuletic, D., Zudin, S., Schelhaas, M.-J. (2023). Significant increase in natural disturbance impacts on European forests since 1950. Global Change Biology, 29, 1359-1376. https://doi.org/10.1111/gcb.16531
2. Forzieri, G., Girardello, M., Ceccherini, G., Spinoni, J., Feyen, L., Hartmann, H., Beck, P. S. A., Camps- Valls, G., Chirici, G., Mauri, A., Cescatti, A. (2021). Emergent vulnerability to climate-driven disturbances in European forests. Nature Communications, 12(1), 1081. https://doi.org/10.1038/s41467-021-21399-7
3. Romagnoli, F., Cadei, A., Costa, M., Marangon, D., Pellegrini, G., Nardi, D., Masiero, M., Secco, L., Grigolato, S., Lingua, E., Picco, L., Pirotti, F., Battisti, A., Locatelli, T., Blennow, K., Gardiner, B., Cavalli, R. (2023). Windstorm impacts on European forest-related systems: an interdisciplinary perspective. Forest Ecology and Management, 541, 121048. https://doi.org/10.1016/j.foreco.2023.121048
4. Catto, J., Ackerley, D., Booth, J., Champion, A. J., Colle, B. A., Pfahl, S., Pinto, J. G., Quinting, J. F., Seiler, C. (2019). The Future of Midlatitude Cyclones. Current Climate Change Reports, 5, 407–420. https://doi.org/10.1007/s40641-019-00149-4
5. Gliksman, D., Averbeck, P., Becker, N., Gardiner, B., Goldberg, V., Grieger, J., Handorf, D., Haustein, K., Karwat, A., Knutzen, F., Lentink, H. S., Lorenz, R., Niermann, D., Pinto, J. G., Queck, R., Ziemann, A. and Franzke, C. L. E. (2023). A European perspective on wind and storm damage – from the meteorological background to index-based approaches to assess impacts. Natural Hazards and Earth System Sciences, 23(6), 2171-2201. https://doi.org/10.5194/nhess-23-2171-2023
6. Giachetti, A., Ferrini, F., Bartoli, G. (2021). A risk analysis procedure for urban trees subjected to wind- or rainstorm. Urban Forestry & Urban Greening, 58, 126941. https://doi.org/10.1016/j.ufug.2020.126941
7. van Haaften, M., Gardebroek, C., Heijman, W., Meuwissen, M. P. M. (2024). Injuries and deaths due to tree failure in The Netherlands: analysis of observational data from 1998–2021. Scientific Reports, 14, 22415. https://doi.org/10.1038/s41598-024-73716-x
8. Gullick, D., Blackburn, G. A., Whyatt, J. D., Vopenka, P., Murray, J., Abbatt, J. (2019). Tree Risk Evaluation Environment for Failure and Limb Loss (TREEFALL): An Integrated Model for Quantifying the Risk of Tree Failure from Local to Regional Scales. Computers, Environment and Urban Systems, 75, 217-228. https://doi.org/10.1016/j.compenvurbsys.2019.02.001
9. Bíl, M., Andrášik, R., Nezval, V., Bílová, M. (2017). Identifying locations along railway networks with the highest tree fall hazard. Applied Geography, 87, 45-53. https://doi.org/10.1016/j.apgeog.2017.07.012
10. Johnson, T. (1996). Strong wind effects on railway operations — 16th October 1987. Journal of Wind Engineering and Industrial Aerodynamics, 60, 251-266. https://doi.org/10.1016/0167-6105(96)00038-4
11. Vajda, A., Tuomenvirta, H., Juga, I., Nurmi, P., Jokinen, P., Rauhala, J. (2014). Severe weather

affecting European transport systems: the identification, classification and frequencies of events. Natural Hazards, 72, 169-188. https://doi.org/10.1007/s11069-013-0895-4
12. Nyberg, R., Johansson, M. (2013). Indicators of road network vulnerability to storm-felled trees. Natural Hazards, 69, 185-199. https://doi.org/10.1007/s11069-013-0693-z
13. Ludvigsen, J., Klæboe, R. (2014). Extreme weather impacts on freight railways in Europe. Natural Hazards, 70, 767–787. https://doi.org/10.1007/s11069-013-0851-3
14. Gardiner, B., Lorenz, R., Hanewinkel, M., Schmitz, B., Bott, F., Szymczak, S., Frick, A., Ulbrich, U. (2024). Predicting the risk of tree fall onto railway lines. Forest Ecology and Management, 553, 121614. https://doi.org/10.1016/j.foreco.2023.121614
15. Hughes, W., Lu, Q., Ding, Z., Zhang, W. (2023). Modeling Tree Damages and Infrastructure Disruptions under Strong Winds for Community Resilience Assessment. ASCE-ASME Journal of Risk and Uncertainty in Engineering Systems, Part A: Civil Engineering, 9(1). https://doi.org/10.1061/AJRUA6.RUENG-956
16. Szymczak, S., Bott, F., Babeck, P., Frick, A., Stöckigt, B., Wagner, K. (2022). Estimating the hazard of tree fall along railway lines: a new GIS tool. Natural Hazards, 112(3), 2237-2258. https://doi.org/10.1007/s11069-022-05263-5
17. Rockel, B., Will, A., Hense, A. (2008). The regional climate model COSMO-CLM (CCLM). Meteorologische Zeitschrift, 17, 347-348. https://doi.org/10.1127/0941-2948/2008/0309
18. Raffaele, L., Bruno, L., Colucci, E. (2024). Reanalysis-based mesoscale wind maps for the design of structures and infrastructures with an application to Italy. Journal of Wind Engineering and Industrial Aerodynamics, 253, 105844. https://doi.org/10.1016/j.jweia.2024.105844
19. Field, C. B., Barros, V., Stocker, T. F., Dahe, Q.J. (2012). Managing the Risks of Extreme Events and Disasters to Advance Climate Change Adaptation: Special Report of the Intergovernmental Panel on Climate Change. Cambridge University Press.
20. Isyumov, N. (2012). Alan G. Davenport's mark on wind engineering. Journal of Wind Engineering and Industrial Aerodynamics, 104–106, 12-24. https://doi.org/10.1016/j.jweia.2012.02.007
21. Picozzi, V., Landi, F., Avossa, A., Croce, P., Formichi, P., Ricciardelli, F. (2024). The climatic action uncertainty chain. Engineering Structures, 301, 117357. https://doi.org/10.1016/j.engstruct.2023.117357
22. Ballio, G., Lagomarsino, S., Piccardo, G., Solari, G. (1999). Probabilistic analysis of Italian extreme winds: Reference velocity and return criterion. Wind & Structure, 2, 51-68. https://doi.org/10.12989/was.1999.2.1.051
23. NTC 2018 (2018). Technical Standards for Construction - Update DM January 17, 2018. Standard, Ministry of Infrastructures and Transport, Rome, Italy.
24. CNR-DT 207 R1/2018 (2018). Guide for the Assessment of Wind Actions and Effects on Structures. Standard, National Research Council (CNR), Rome, Italy.
25. Orlanski, I. (1975). A rational subdivision of scales for atmospheric processes. Bull. Am. Meteorol. Soc., 56, 527–530.
26. Dyrbye, C. and Hansen, S. O. (1996), Wind loads on structures. Wiley.
27. Hersbach, H., Bell, B., Berrisford, P., Hirahara, S., Horányi, A., Muñoz Sabater, J., Nicolas, J., Peubey, C., Radu, R., Schepers, D., Simmons, A., Soci, C., Abdalla, S., Abellan, X., Balsamo, G., Bechtold, P., Biavati, G., Bidlot, J., Bonavita, M., De Chiara, G., Dahlgren, P., Dee, D., Diamantakis, M., Dragani, R., Flemming, J., Forbes, R., Fuentes, M., Geer, A., Haimberger, L., Healy, S., Hogan, R.J., Hólm, E., Janisková, M., Keeley, S., Laloyaux, P., Lopez, P., Lupu, C., Radnoti, G., de Rosnay, P., Rozum, I., Vamborg, F., Villaume, S. and Thépaut, J.N. (2020). The ERA5 global reanalysis. Quarterly Journal of the Royal Meteorological Society, 146, 1999-2049. https://doi.org/10.1002/qj.3803
28. Yang, S., Chouinard, L.E., Langlois, S. (2022). Hourly wind data for aeolian vibration analysis of overhead transmission line conductors. Journal of Wind Engineering and Industrial Aerodynamics, 230, 105184. https://doi.org/10.1016/j.jweia.2022.105184.
29. Raffa, M., Reder, A., Marras, G.F., Mancini, M., Scipione, G., Santini, M., Mercogliano, P. (2021). VHR-REA_IT dataset: Very high resolution dynamical downscaling of ERA5 reanalysis over Italy by COSMO-CLM. Data 6(8), 88. https://doi.org/10.3390/data6080088

30. Raffa, M., Adinolfi, M., Reder, A., Marras, G. F., Mancini, M., Scipione, G., Santini, M., Mercogliano, P. (2023). Very high resolution projections over Italy under different CMIP5 IPCC scenarios. Scientific Data, 10(1), 238. https://doi.org/10.1038/s41597-023-02144-9
31. Belušić Vozila, A., Belušić, D., Telišman Prtenjak, M., Güttler, I., Bastin, S., Brisson, E., Demory, M.E., Dobler, A., Feldmann, H., Hodnebrog, Ø., Kartsios, S., Keuler, K., Lorenz, T., Milovac, J., Pichelli, E., Raffa, M., Soares, P.M.M., Tölle, M.H., Truhetz, H., de Vries, H., Warrach-Sagi, K. (2024). Evaluation of the near-surface wind field over the Adriatic region: local wind characteristics in the convection-permitting model ensemble. Climate Dynamics, 62(6), 4617-4634. https://doi.org/10.1007/s00382-023-06703-z
32. Hastings, D., Dumbar, P., Elphingstone, G., Bootz, M., Murakami, H., Maruyama, H., Masaharu, H., Holland, P., Payne, J., Bryant, N., Logan, T., Murre, J., Schreier, G., MacDonald, J. (1999). The Global Land One-Kilometer Base Elevation (GLOBE) Digital Elevation Model. National Oceanic and Atmospheric Administration, National Geophysical Data Center, 325 Broadway, Boulder, Colorado 80305-3328, U.S.A, Version 1.0. http://www.ngdc.noaa.gov/mgg/topo/globe.html
33. Bartholomé, E., Belward, A. (2005). GLC2000: A new approach to global land cover mapping from earth observation data. International Journal of Remote Sensing 26, 1959-1977. http://doi.org/10.1080/01431160412331291297
34. Dolce, M., Prota, A., Borzi, B., da Porto, F., Lagomarsino, S., Magenes, G., Moroni, C., Penna, A., Polese, M., Speranza, E., Verderame, G. M., Zuccaro, G. (2021). Seismic risk assessment of residential buildings in Italy. Bulletin of Earthquake Engineering, 19, 2999–3032. https://doi.org/10.1007/s10518-020-01009-5
35. Mitchell, S. J. (2013). Wind as a natural disturbance agent in forests: a synthesis. Forestry, 86, 147-157. https://doi.org/10.1093/forestry/cps058
36. Gardiner, B., Peter, B., Moulia, B. (2016). Review: Wind impacts on plant growth, mechanics and damage. Plant Science, 245, 94-118. https://doi.org/10.1016/j.plantsci.2016.01.006
37. Peltola, H., Kellomäki, S., Väisänen, H., Ikonen, V.-P. (1999), A mechanistic model for assessing the risk of wind and snow damage to single trees and stands of Scots pine, Norway spruce, and birch. Canadian Journal of Forest Research, 29(6), 647-661. https://doi.org/10.1139/x99-029
38. Gardiner, B., Peltola, H., Kellomäki, S. (2000). Comparison of two models for predicting the critical wind speeds required to damage coniferous trees. Ecological modelling, 129(1), 1-23. https://doi.org/10.1016/S0304-3800(00)00220-9
39. Ancelin, P., Courbaud, B., Fourcaud, T. (2004). Development of an individual tree-based mechanical model to predict wind damage within forest stands. Forest Ecology and Management, 203(1-3), 101-121. https://doi.org/10.1016/j.foreco.2004.07.067
40. Ciftci, C., Brena, S. F., Kane, B., Arwade, S. R. (2013). The effect of crown architecture on dynamic amplification factor of an open-grown sugar maple (Acer saccharum L.). Trees - Structure and Function, 27(4), 1175-1189. https://doi.org/10.1007/s00468-013-0867-z
41. Ciftci, C., Arwade, S. R., Kane, B., Brena, S. F. (2014a). Analysis of the probability of failure for open-grown trees during wind storms. Probabilistic Engineering Mechanics, 37, 41-50. https://doi.org/10.1016/j.probengmech.2014.04.002
42. Jackson, T., Shenkin, A., Wellpott, A., Calders, K., Origo, N., Disney, M., Burt, A., Raumonen, P., Gardiner, B., Herold, M., Fourcaud, T., Malhi, Y. (2019) "Finite element analysis of trees in the wind based on terrestrial laser scanning data". Agricultural and Forest Meteorology, 265, 137-144. https://doi.org/10.1016/j.agrformet.2018.11.014
43. Hou, G., Chen, S. (2020). Probabilistic modeling of disrupted infrastructures due to fallen trees subjected to extreme winds in urban community. Natural Hazards, 102(3), 1323-1350. https://doi.org/10.1007/s11069-020-03969-y
44. Lopez, D., Michelin, S., de Langre, E. (2011). Flow-induced pruning of branched systems and brittle reconfiguration. Journal of Theoretical Biology, 284, 117-124. https://doi.org/10.1016/j.jtbi.2011.06.027
45. Garrat, J. R. (1992). The atmospheric boundary layer. Cambridge University Press, New York, USA.
46. Floors, R., Enevoldsen, P., Davis, N., Arnqvist, J., Dellwik, E. (2018). From lidar scans to roughness

maps for wind resource modelling in forested areas. Wind Energy Science, 3, 353-370. https://doi.org/10.5194/wes-3-353-2018
47. Crowther, T. W., Glick, H. B., Covey, K. R., Bettigole, C., Maynard, D. S., Thomas, S. M., Smith, J. R., Hintler, G., Duguid, M. C., Amatulli, G., Tuanmu, M. N., Jetz, W., Salas, C., Stam, C., Piotto, D., Tavani, R., Green, S., Bruce, G., Williams, S. J., Wiser, S. K., Huber, M. O., Kattge, J., Reich, P. B., Bradford, M. A. (2015). Mapping tree density at a global scale. Nature, 525, 201–205. https://doi.org/10.1038/nature14967
48. Lang, N., Jetz, W., Schindler, K., Wegner, J. D. (2023). A high-resolution canopy height model of the Earth. Nature Ecology & Evolution, 7, 1778-1789. https://doi.org/10.1038/s41559-023-02206-6
49. CLC 2018 (2020). CORINE Land Cover 2018 (Vector), Europe, 6-Yearly - Version 2020 20u1, May 2020. Technical Report. https://land.copernicus.eu/en/products/corine-land-cover/clc2018
50. Ferrovieincalabria.it (2019). Maltempo estremo e ritardi infiniti: ci dovremo abituare, ma… https://www.ferrovieincalabria.it/maltempo-estremo-e-ritardi-infiniti-ci-dovremo-abituare-ma/
51. ANSA.it (2025). Maltempo causa disagi per circolazione treni nel cosentino. https://www.ansa.it/sito/notizie/cronaca/2025/01/17/maltempo-causa-disagi-per-circolazione-treni-nel-cosentino_7e8fdff5-af7e-49dd-88ca-5baaf7dfad46.html
52. Miocomune.tv (2025). Maltempo in Calabria, a Fuscaldo forte vento: attiva la protezione civile. https://www.miocomune.tv/post/maltempo-in-calabria-a-fuscaldo-forte-vento-attiva-la-protezione-civile
53. Lacnews24.it (2025). Albero cade sui binari a Belvedere Marittimo per il forte vento: sulla linea Paola-Sapri ritardi e treni a velocità ridotta. https://www.lacnews24.it/cronaca/albero-cade-sui-binari-a-belvedere-marittimo-per-il-forte-vento-sulla-linea-paola-sapri-ritardi-e-treni-a-velocita-ridotta-b9qmx4r6
54. Napoli.corriere.it (2025). Maltempo Sud Italia, cosa sta succedendo in Calabria, Sicilia e Campania: le ultime notizie in diretta. https://napoli.corriere.it/cronaca/diretta-live/25_gennaio_14/maltempo-sud-italia-live-calabria-sicilia-campania.shtml?utm_
55. Hou, G., Chen, S. (2020). Probabilistic modeling of disrupted infrastructures due to fallen trees subjected to extreme winds in urban community. Natural Hazards, 102(3), 1323-1350. https://doi.org/10.1007/s11069-020-03969-y